

# Tectonics

## RESEARCH ARTICLE

10.1029/2019TC005806

### Key Points:

- Kingston Harbor preserves records of Pleistocene to present blind faults
- The Harbor faults are an extension of an onshore strike-slip fault in Southeast Jamaica
- Fault reactivating may generate a  $M_w$  5.8–6.9 earthquake

### Supporting Information:

- Supporting Information S1

### Correspondence to:

V. Wright,  
vdwright@smu.edu

### Citation:

Wright, V., Hornbach, M., Brown, L., McHugh, C., & Mitchell, S. (2019). Neotectonics of Southeast Jamaica derived from marine seismic surveys and gravity cores. *Tectonics*, 38. <https://doi.org/10.1029/2019TC005806>

Received 2 AUG 2019

Accepted 4 NOV 2019

Accepted article online 13 NOV 2019

©2019. The Authors.

This is an open access article under the terms of the Creative Commons Attribution License, which permits use, distribution and reproduction in any medium, provided the original work is properly cited.

## Neotectonics of Southeast Jamaica Derived From Marine Seismic Surveys and Gravity Cores

Vanshan Wright<sup>1</sup> , Matthew Hornbach<sup>1</sup>, Lyndon Brown<sup>2</sup>, Cecilia McHugh<sup>3</sup> , and Simon Mitchell<sup>2,4</sup>

<sup>1</sup>Roy Huffington Department of Earth Sciences, Southern Methodist University, Dallas, TX, USA, <sup>2</sup>The Earthquake Unit, The University of the West Indies, Kingston, Jamaica, <sup>3</sup>School of Earth and Environmental Sciences, Queens College, New York, NY, USA, <sup>4</sup>Department of Geography and Geology, The University of the West Indies, Kingston, Jamaica

**Abstract** Tectonics in Southeast Jamaica is poorly understood, but the region may contain currently unknown faults that could generate large-magnitude earthquakes. This study constrains tectonics in Southeast Jamaica by collecting and analyzing seismic and shallow sediment core data in and around Kingston Harbor. Seismic results reveal a previously unrecognized strike-slip fault system that accommodates strain via a complex mix of compression and extension. The faults appear to be a blind extension of one major fault (i.e., The Bull Bay Strike-Slip Fault) within the Enriquillo-Plantain Garden Fault Zone. This fault system may represent significant hazards to Kingston Jamaica because the fault is active, located less than 5 km from the city, and a complete rupture of the fault could generate a  $M_w$  5.8–6.9 earthquake. Our analyses highlight the need for continued paleoseismic studies, both onshore and offshore Jamaica.

### 1. Introduction

Jamaica experiences transpression due to oblique convergence between the Gonave Microplate and Caribbean Plate, whose plate boundary bisects the island (Figure 1; Benford et al., 2012; Mann et al., 1985; Rosencrantz & Mann, 1991). The Gonave-Caribbean boundary is defined by the Enriquillo-Plantain Garden Fault Zone (EPGFZ) in the east and the Walton Fault Zone (WFZ) in the west (Figure 1; Horsfield, 1974; Mann et al., 1985). Seismicity is greatest in the east where the EPGFZ (DeMets & Wiggins-Grandison, 2007; Salazar et al., 2013; Wiggins-Grandison, 2001; Wiggins-Grandison & Atakan, 2005) manifests as a broad and tectonically complex flower structure (Figure 1; Mann et al., 1985; Mann et al., 2007; James-Williamson et al., 2014). Fault zone deformation mainly includes thrusting and folding within several thrust mountains in eastern Jamaica (e.g., the Wagwater, Dallas, Long, and Blue Mountains) and sinistral motion along the Plantain Garden and Cavaliers faults, which define the main plate boundary (i.e., the EPGF; Figure 1). Though the EPGF is thought to be the primary source for large magnitude ( $>M_w$  6) earthquakes, moderate to large earthquakes (e.g., 2010  $M_w$  7 Haiti event) may have also occurred along previously unknown, blind, or poorly constrained faults that accommodate strain from the EPGF (Bakun et al., 2012; Hayes et al., 2010; Koehler et al., 2013; Wiggins-Grandison & Atakan, 2005). Recent studies also show that deformation is often concentrated along blind fault systems that are either adjacent to, extend away from, or connect at depth with the EPGF (e.g., Corbeau et al., 2016; Wang et al., 2018).

Currently, few data exist to constrain the location of active blind or buried faults in Jamaica. Fault masking occurs because steep or rugged terrain, sedimentation, vegetation, and human development limit fault exposure (Koehler et al., 2013). In cases where faults are exposed and mappable, erosion and lack of age-dating data often compromise efforts to estimate tectonic deformation rates (Koehler et al., 2013). Field observations are sometimes supplemented with campaign GPS data, but tectonic deformation constrained from these studies often has relatively high uncertainties due to the limited spatial and temporal coverages of the GPS networks used (e.g., Benford et al., 2012; DeMets & Wiggins-Grandison, 2007). Studies relying on passive source seismic data also produce first-order tectonic deformation results due to the limited spatial coverage of the seismographs whose data analyses often result in kilometer-scale earthquake location uncertainties, poorly constrained velocity models, and few high-quality focal mechanisms (DeMets & Wiggins-Grandison, 2007; Wiggins-Grandison & Atakan, 2005).

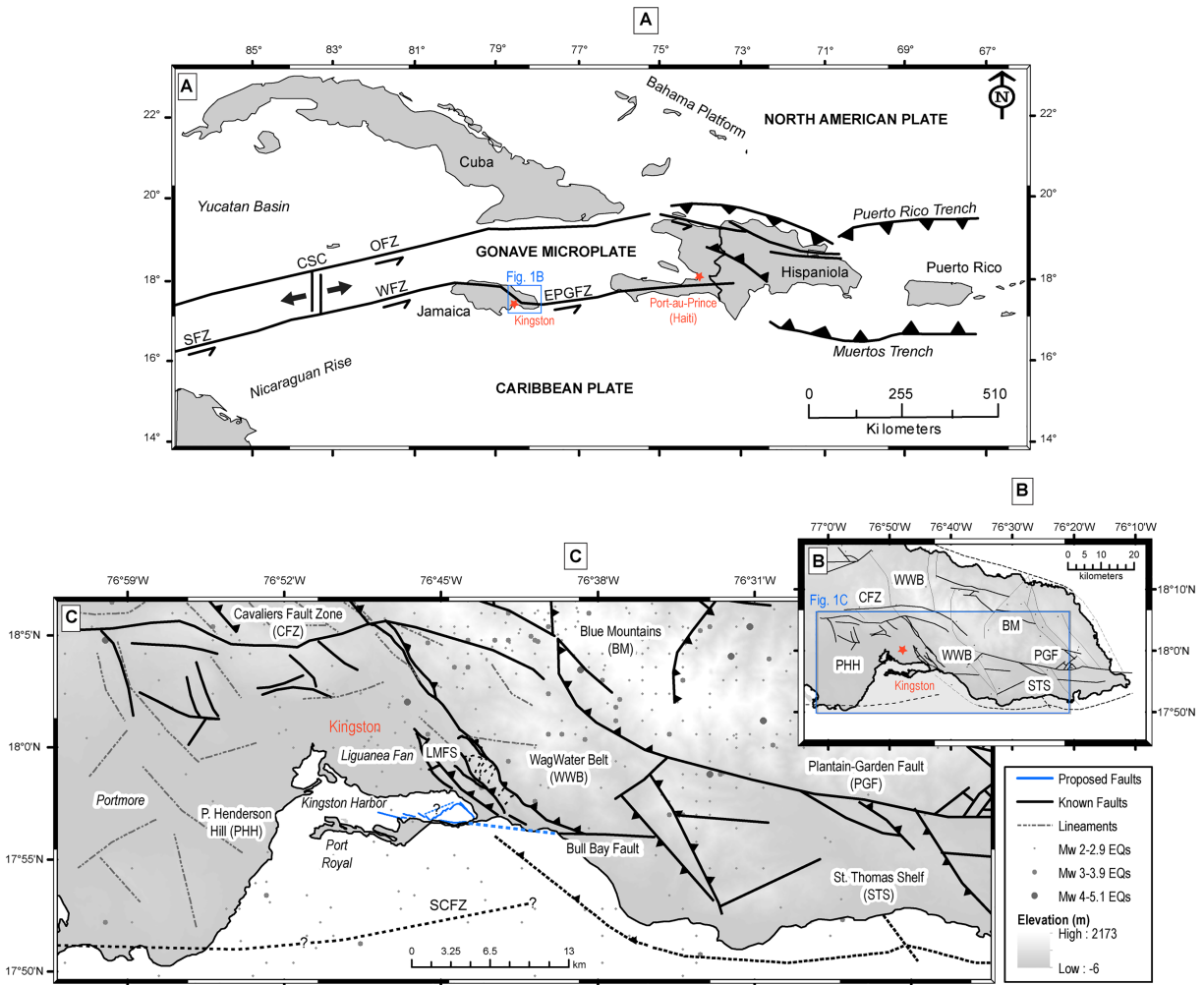


**Figure 1.** (a) Regional map shows that Jamaica is bisected by the Caribbean plate and the Gonave Microplate. The country experiences intraplate shearing as a result. Map also shows the locations for the major plates in the region. These plates are bounded by the Enriquillo-Plantain Garden Fault Zone (EPGFZ), the Walton Fault Zone (WFZ), the Oriente Fault Zone (OFZ), and the Cayman Spreading Center (CSC). (b) Map of Eastern Jamaica showing the locations of mapped faults and major tectonic structures that create the restraining bend flower structure. The abbreviation LMFS refers to the Long Mountain Fault System, which comprises of the Long and Dallas Thrust Mountains (see Figure 2a). Fault locations are adopted from Wiggins-Grandison and Atakan (2005), Benford et al. (2012), and James-Williamson et al. (2014). (c) The figure is a more zoomed-in map (blue box in Figure 1b), showing the faults, lineaments, and earthquakes locations in the region.

One way to better constrain subsurface fault geometry and paleoseismic deformation is through the collection and integration of active source seismic data and sediment cores. Marine seismic-reflection profiles show that the EPGF follows a clear linear bathymetric trend east of Jamaica (e.g., Corbeau et al., 2016). Seismic-reflection profiles also show that extensional faults are present offshore, south of Kingston Jamaica (Figure 1; Burke, 1967; Hornbach et al., 2011). To date, the age of the EPGF and its connections with onshore faults remain unclear. Further, seismic imaging and sediment core dating above or near these offshore extensional faults can, however, provide a way to place age constraints on tectonic deformation.

Our study addresses the relationship between onshore and offshore faults in the tectonically complex region of southeast Jamaica, near Kingston (Figure 1). It builds upon the works of Burke (1967) and Hornbach et al. (2011) by supplementing their data sets with ~260 km of additional seismic-reflection data within the Kingston Harbor and age-dating constraints from seismic, sediment core, and sea level curve analyses (Figure 1). Our results suggest that Kingston Harbor contains an active offshore strike-slip fault system that likely accommodates strain from an onshore fault (i.e., the Bull Bay strike-slip fault) associated with EPGFZ. Empirical relationships between earthquake magnitude and length (Wells & Coppersmith, 1994) indicate that the newly identified fault system could generate large ( $M_w$  5.8–6.9) earthquakes.

## 2. Tectonic and Geomorphic Background

### 2.1. Tectonic Evolution of the EPGFZ in Eastern Jamaica

The EPGFZ is narrow and well-defined offshore Jamaica (Corbeau et al., 2016) but poorly constrained on the island where the fault zone manifests as a flower structure that has been expanding southwestward since the middle Miocene (Figure 1; Horsfield, 1974; James-Williamson et al., 2014; Mann et al., 1985; Mann et al., 2007; Wadge & Dixon, 1984). By the middle to late Miocene, submarine extensional half-grabens were actively subsiding in eastern Jamaica (Horsfield, 1974; Mann et al., 1985; Wadge & Dixon, 1984). Middle Miocene to early Pliocene sinistral motion and transpression along the Plantain-Garden fault (including the interactions between the westward moving Gonave Microplate and preexisting structures in eastern Jamaica) created a sigmoidal-shaped fault zone that hosted an uplifted fold and thrust structure (i.e., the Proto-Blue Mountain) at its center (Figure 1; James-Williamson et al., 2014). Uplift within Proto-Blue Mountain dynamically loaded and caused subsidence within the region to the south (i.e., the St. Thomas Shelf; Figure 1; James-Williamson et al., 2014). Continued early Pliocene to early Pleistocene transpression eventually led to a southwestward extension of the sigmoidal fault zone. Its new boundary developed along the northwest trending reverse faults that define the western edge of the Wagwater Belt and along an inferred west-east trending strike-slip fault in offshore southern Jamaica (Figure 1; James-Williamson et al., 2014). Strain accommodation within the fault zone likely included inversion, uplift, and subaerial exposure of the structures within the Wagwater Belt and St. Thomas Shelf (Figure 1; Mann et al., 1985; Mann et al., 2007; James-Williamson et al., 2014).

Since the late Pleistocene, deformation within the EPGFZ has been dominated by thrust faulting and continued strike slip, including along the Cavaliers and Plantain-Garden faults, which now represents EPGF—that is, the main plate boundary fault (Figure 1; Horsfield, 1974; James-Williamson et al., 2014; Mann et al., 1985; Mann et al., 2007; Wadge & Dixon, 1984). Strike-slip faulting may have also stepped southward along an active fault that trends subparallel to the Palisadoes Complex Spit—herein referred to as the Bull Bay Strike-Slip Fault (Figure 1; James-Williamson et al., 2014). Active thrusting has continued within the Blue Mountain and Wagwater Belt, where average uplift rates of 1–2 mm/year have occurred since the late Miocene (Cochran et al., 2017). Based on analyses of trace element data, field mapping surveys, and thermodynamic calculations, Abbott et al. (2016) suggest that Holocene aged uplift may also exist at Port Henderson Hill, located ~40 km southwest of the Blue Mountain (Figure 1).

Current uncertainties for the EPGFZ include, but are not limited to, the nature of the South Coastal sinistral fault zone (SCFZ) and the Long Mountain fault system (LMFS; Figure 1). The SCFZ exhibits evidence for left-lateral deformation on land in Southcentral Jamaica (Koehler et al., 2013), but its offshore trend and timing of latest activity are currently unclear. Based on bathymetric, passive source seismic, and geodetic data, some studies hypothesize that the SCFZ continues offshore (i.e., South Central and Eastern Jamaica; Figure 1) and that motion along faults within the SCFZ likely contributes to active deformation within the EPGFZ (e.g., Benford et al., 2012; Draper, 2008). To date, the SCFZ's age, rate of motion, and relationship with on-land faults in eastern Jamaica are poorly constrained. While Benford et al. (2012) suggest that the onshore fault systems cause shortening offshore Kingston, their results contrast with Burke (1967) and Hornbach et al. (2011), who provide evidence for active normal faulting. Draper (2008) and Hornbach et al. (2011) interpret a scarp along the western edge of the LMFS as a west dipping normal fault (i.e., the Long Mountain Fault). Hornbach et al. (2011) inferred (using marine seismic data) that this normal fault extends through the northeast corner of the Kingston Harbor.

Together, the limited existing data indicate that active deformation is concentrated not only on relatively older structures such as the Blue Mountains, Wagwater Belt, and the Plantain Garden Fault but also along Holocene structures located between the Cavaliers Fault and SCFZ—that is, within the Kingston Region. A more detailed tectonic analysis of the Kingston Harbor area (Figures 1 and 2) is, therefore, expected to provide insight into the evolution and tectonics of eastern Jamaica.

### 2.2. Evolution of the Kingston Harbor Area

The shallow marine environment south of Kingston Harbor (Figure 2) likely developed in five stages (Goreau & Burke, 1966). (1) During the Sangamonian (~80 to 125 ka), the region hosted carbonate platforms that grew while sea level was high (Goreau & Burke, 1966; Steers, 1940). (2) Subsequent interglacial sea level

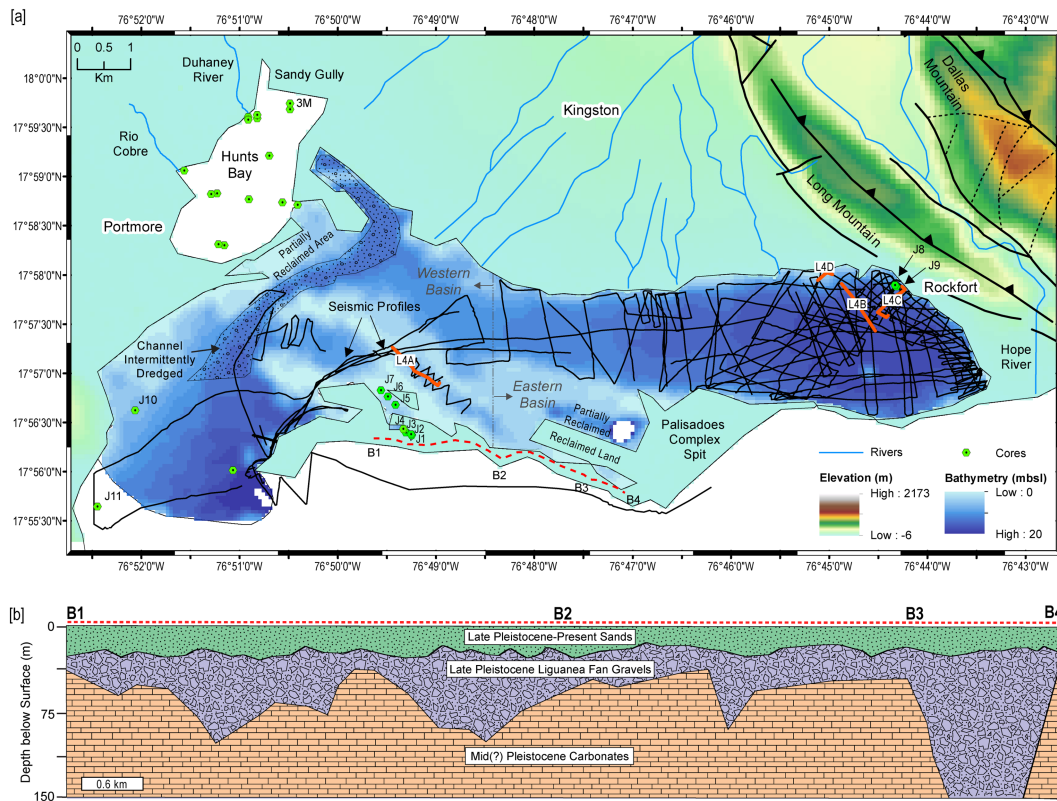


**Figure 2.** (a) Map shows the Kingston Harbor and Hunts Bay. The map also shows drainages that supply sediments to the Harbor and Hunts Bay and collection sites for all 2-D seismic profiles and sediment cores. The images of the red-orange highlighted seismic lines are shown in Figure 4, where they are labeled as Lines 4A-D (L4A-D). The red dashed line along the tombolo represents the location of a refraction survey line (Goreau & Burke, 1966). (b) This schematic shows Goreau and Burke (1966)'s interpretation of the refraction survey line (red dashed line in Figure 2a). The lowermost layer corresponds to Pleistocene carbonates that were deposited in conjunction with rising sea levels. The middle layer is the late-Pleistocene aged Liguanea fan gravels that prograded across the region, and the topmost layer is sandy sediments.

low stands lead to erosion of the carbonate platforms down to ~40 m below sea level (mbsl; Goreau & Burke, 1966). During this time and likely afterward, the Liguanea Fan—fed by the Hope River—prograded up to ~2 km south of the current position of the Palisadoes Complex Spit (Figure 2; Goreau & Burke, 1966). (3) The migration of the fan halted when the Hope River was diverted eastward between Dallas and Long Mountains, whose uplift likely initiated the river's diversion (Goreau & Burke, 1966; Draper, 2008). (4) As sea levels rose near the end of the late Pleistocene, sediments deposited offshore by the Hope River were transported westward via longshore drift (Goreau & Burke, 1966). Some sediments were captured by carbonate reefs and gravels that extended westward from the protruding edge of the island that currently connects the Palisadoes Complex Spit to the mainland (Goreau & Burke, 1966; Steers, 1940). (5) Continued late Pleistocene to present sea level rise and sediment capture created the Palisadoes Complex Spit, which began as a sand spit that eventually connected to the island known as Port Royal (Steers, 1940; Goreau & Burke, 1966; Figure 2).

Currently, the Harbor is connected to a shallow inlet known as Hunt's Bay (Figure 2). Both water bodies receive sediments from fluvial channels, human-made gullies, overland flow, and wind (Andrews et al., 1998). Sediments within the upper 100 cm of Hunts Bay (Figure 2) are mostly nonlaminated muds and silts (Figure 3). Sedimentation rates in the northeastern section of Hunts Bay are relatively high (6 cm/year for the upper 70 cm; Andrews et al., 1998). The southwestern section of the Harbor contains mostly sands (Andrews et al., 1998). There are no known (to our knowledge) direct estimates for sedimentation rates in the Harbor.

The Harbor and Hunts Bay sediments have been influenced by dredging and engineered land reclamation. To allow ships to enter the Harbor, the Jamaican government has repeatedly (at least three times since 1970)

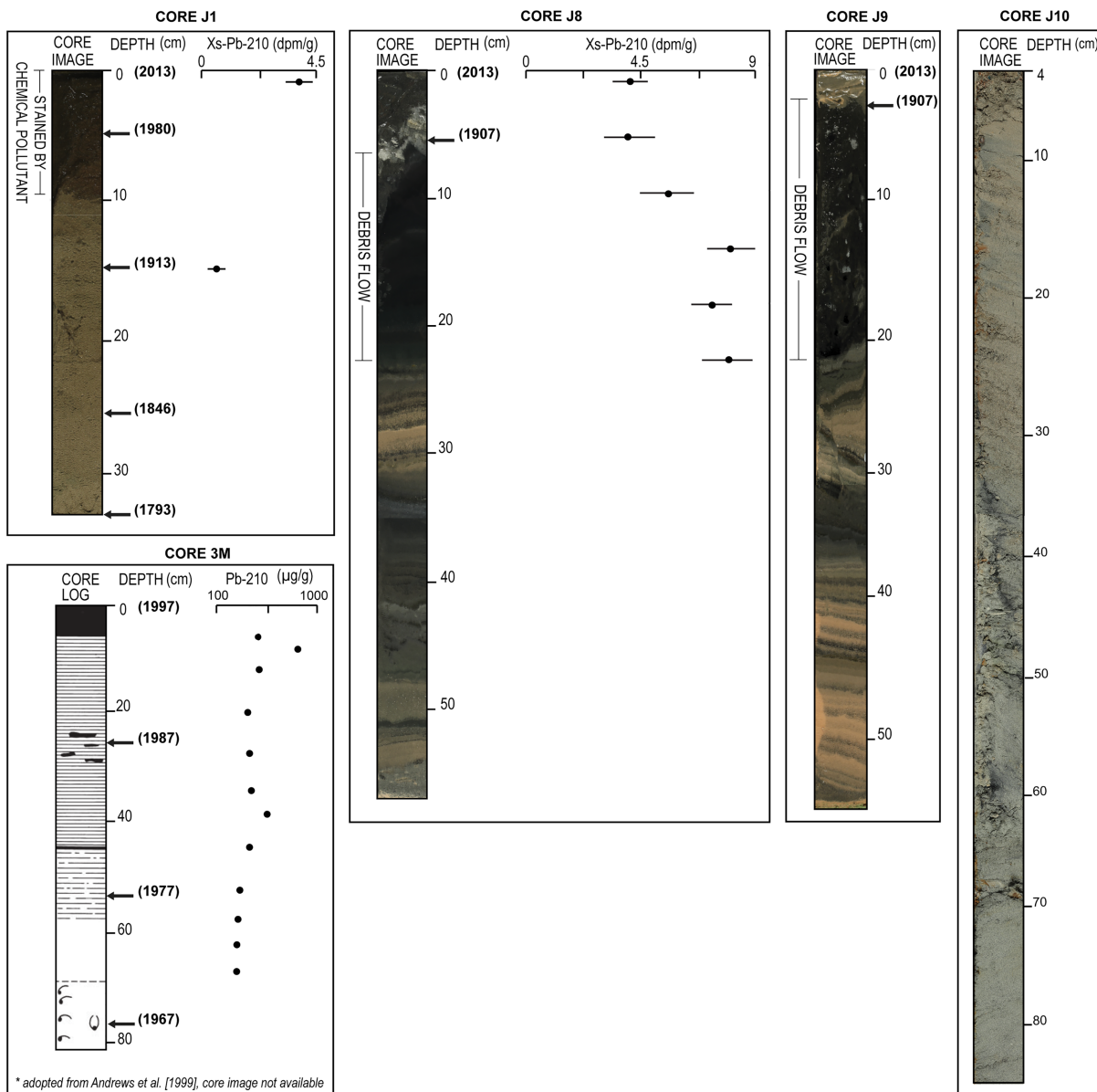


**Figure 3.** Images show five cores collected within the Kingston Harbor and Hunts Bay. Pb-210 analyses were conducted on three of the cores. Core collection locations are shown in Figure 2a.

dredged the narrow channel within the western section of the Harbor (Goodbody, 2003; also see Figure 2). Dredged sediments are often dumped on either side of the bank of the submarine channel (i.e., within a few meters of the channel). Jamaica's government has also reclaimed the previous section of the Harbor (via artificially engineered landfilling) that now host the Airport located on the Palisades Complex Spit (Figure 2). Though some sediments are stained by chemical pollutants (Figure 3), we found no other known reports of significant anthropogenic activities that would likely influence the structure of the sediment within the Harbor.

Relatively little is known about the effects of natural disasters and geologic events (e.g., earthquakes, hurricanes, and currents) on the Harbor sediments. Although hurricanes have eroded and transported sediments on the seaward side of the Palisades Complex Spit, there are no known reports of hurricane-induced slope failure, erosion, or sediment disturbances/depositions within the Harbor. In contrast, previous studies report that the 1692 ( $M_w$  6.5–7) and 1907 ( $M_w$  6–6.5) Jamaican earthquakes have caused subsidence of the Harbor

floor though the exact subsidence locations have not been mapped (e.g., Sloane et al., 1694; Fuller, 1907). It is also unclear when and to what degree active faulting within the Harbor has deformed its sediments (Hornbach et al., 2011).

### 3. Approach for Assessing Tectonic Deformation

We assess tectonics and sedimentation in the Harbor by collecting and analyzing sediment cores and active source seismic data (Figure 2). We use the cores (Figure 3) to constrain patterns and rates of recent sedimentation and use seismic data, along with existing geologic data, to provide relative and absolute dates of sediments and to infer tectonic deformation (Figures 4–8). After that, we integrate seismic and core data with results from existing field mapping studies to assess the relationship between offshore and onshore faults in Eastern Jamaica.

#### 3.1. Coring Data Collection and Analyses

We collected 11 short (33–100 cm) sediment cores (named J1–J11 in Figure 2) using either metal push corers or plastic gravity cylinder corers that freefall through the water column (Figure 2 for locations). Seven (J1–J7) are 33–100 cm long gravity cores collected in the south central section of the Harbor; two cores (J8 and J9) are ~60 cm long gravity cores collected in the northeastern section of the Harbor, and the final two (J10 and J11) are ~100 cm long push cores collected in the southwestern section of the Harbor.

We capped and shipped cores J1–J9 and J10–J11 to Lamont-Doherty Earth Observatory and Texas A&M University, respectively. There, we split each core vertically and described the grain size, Munsell color, bioturbation zones, sedimentary structures, bed thickness, and apparent dip, and the nature of the contact between beds (i.e., whether the contacts between the beds are conformable, sharp, gradation, and wavy). We also estimated sedimentation rates using excess (xs) Pb-210 isotope dating of sediments in cores J1 and J8. For this, we calculated a deposition rate that is equal to the product of the Pb-210 radioactive decay constant ( $0.0311 \text{ year}^{-1}$ ) and the rate of change in the base 10 log of the excess Pb-210 as a function of cumulative sediment thickness. We estimate the excess Pb-210 (in disintegrations per minute per gram (dpg/m)) using a nondestructive gamma ray bombardment analysis done with partially full-tube and full-tube efficiencies for cores J1 and J8, respectively, and we used the least squares method to linearly fit the log<sub>10</sub> excess Pb-210 versus cumulative sediment thickness curves. The resulting sedimentation rates represent averages (because of the linear fit) and are herein reported with 1-sigma (68.2%) uncertainties. While using sedimentation rates to constrain sediment age, we assumed that sediments at the top of the core were deposited in 2013—that is, the year we collected the cores. We made this assumption because Cs-137 analyses showed no detectable radioactivity (possibly due to the low latitude and saline waters) and Be-7 data were not available.

#### 3.2. Seismic Data Collection and Analyses

We collected a total of ~260 km of seismic-reflection profiles during three multiyear campaigns between 2009 and 2013 (Figure 2). Data were collected using a Knudsen 3212 single-channel, zero-offset subbottom profiler, which uses a sweep frequency source (i.e., chirp with a center frequency of 3.5 kHz) and match filtering to process seismic data (e.g., Henkart, 2006). The system records seismic data in the SEG-Y format, and an internal GPS constrains each shot and receiver position to within  $\pm 5$  m.

We loaded all data in Kingdom 2015 software, converted from two-way traveltimes to depth assuming a compressional wave velocity of 1,500 m/s, and plotted the data using amplitude, Hilbert, envelope, and average energy seismic attributes. We traced and created two-dimensional natural neighbor interpolated maps of the main seismic horizons, identified erosional unconformities, examined groups of reflections whose dips deviate significantly from horizontal, and created isopach maps for seismically distinguishable sedimentary units. We used results from these analyses to both relatively date sediments using principles of superposition and crosscutting relations and to ascribe absolute dates to sediments by associating anomalous (i.e., steeply dipping) reflector packages with already dated geologic events in Jamaica's past.

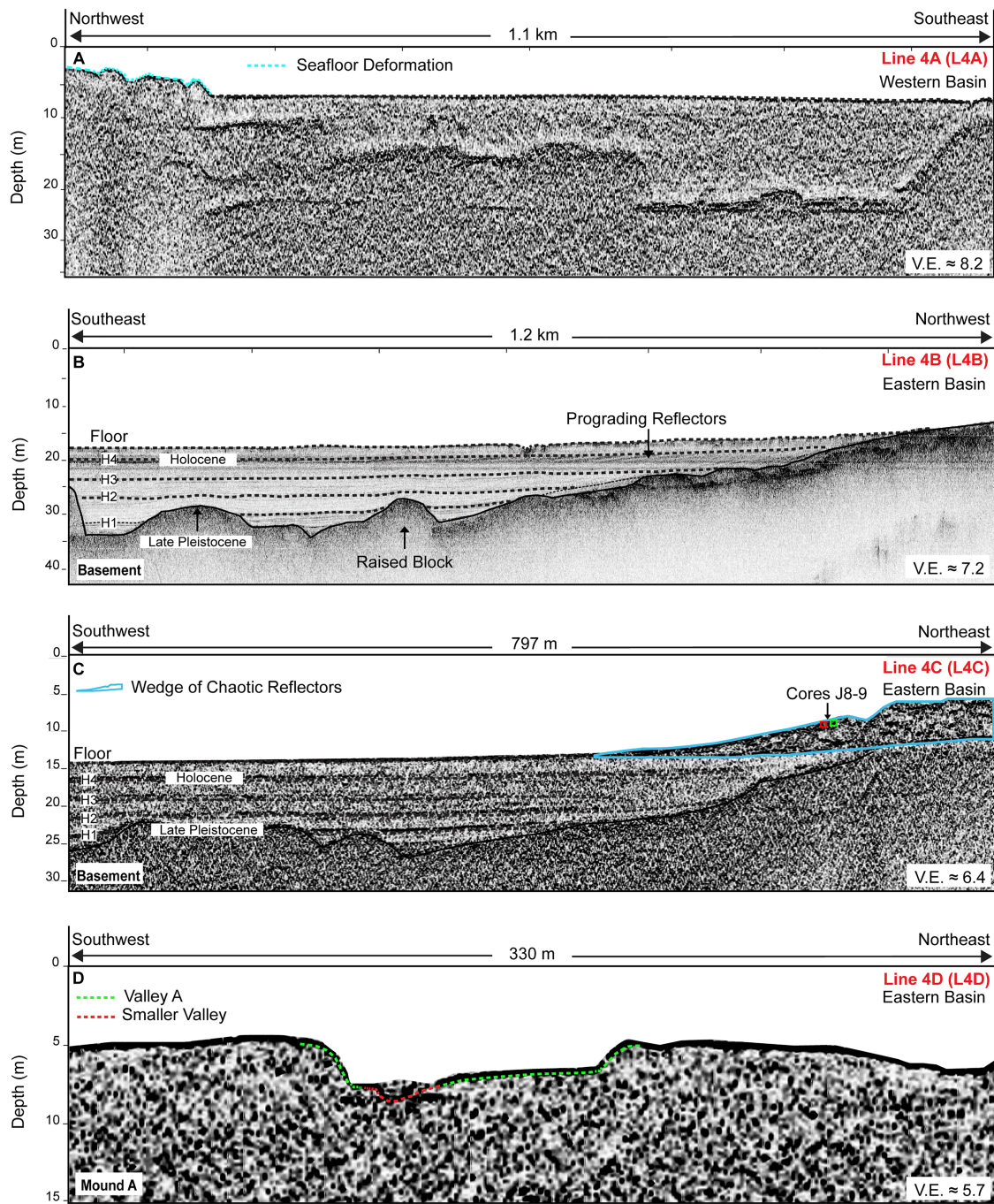


**Figure 4.** (a) Seismic image shows the typical reflectivity observed in the western basin of the Harbor—that is, the Harbor floor sometimes creates a masking effect that prevents deeper penetrating continuous reflectors. (b) The seismic image shows the four main horizons, a wedge of prograding reflections, and erosional unconformity. (c) The seismic image shows a wedge-shaped group of sediments that produces shallow chaotic seismic reflectivity. It also shows the four main horizons in the Harbor. The wedge-shaped group of sediments most probably represents a group of mass wasting deposits. The red and green rectangles show approximate locations for cores J8–J9. (d) The seismic profile shows an example of the valleys and sea mounds in the Harbor. The areal extent of each feature in (a)–(c) is shown in Figure 5. The four main seismic horizons (Figures 4a, 4b, and 5) and two erosional unconformities (Figure 4a) provide information for relative sediment ages. Horizon 1–4 extends across the eastern Harbor, although some are not continuously traceable across the entire basin (Figure 5). The horizons generally have subhorizontal apparent dips (average =  $0.1^\circ$ ), terminate against the basement (including the margins of the triangular platforms), lack significant undulation, and deepen southeastward (Figure 5). The two erosional unconformities are between horizons 2 and 3 (Figure 4a). One is between 17.4 and 21 mbsl and restricted to the northeastern section of the Eastern Harbor (below prograding clinofolds—see Figures 4b and 5) where it spans an area of  $147,883 \text{ m}^2$ . The second is between 18 and 21 mbsl and restricted to the easternmost section of the Eastern Harbor, where it spans an area of  $940,362 \text{ m}^2$ . The abbreviation V.E. refers to vertical exaggeration.

#### 4. General Basin Stratigraphy and Age-Dating Results

Kingston Harbor can be divided into two basins, which display distinctive bathymetric, sedimentary, and seismic properties (Figures 2–5). The basins are herein referred to as the western and eastern basins (Figure 2). The western basin has an irregular bathymetry and includes a narrow channel that allows ships to enter the Harbor (Figure 2). In the western basin, the Harbor floor creates a zone of transparency and acoustic masking that sometimes prevents deep-penetrating continuous return reflections (Figure 4a). Sediments within the upper 100 cm of the westernmost section of the eastern basin are medium- to coarse-grained sands and gravels interspersed with shell fragments (see CJ10 in Figure 3). Vacuoles are also relatively common, but it is unclear whether they are natural, caused by sediment dredging or disturbances during coring (see CJ10 in Figure 3). Sediments toward the southeastern section of the western basin contain a mix of fine- to medium-grained sands (see CJ1 in Figure 3). Excess Pb-210 within Core J1 (collected in the western basin) decreases from 3.18–4.34 dpg/m to 0–0.58 dpg/m (Figure 3). This yields an average sedimentation rate of 0.1–0.2 cm/year for the upper 14 cm; however, with only two points, the uncertainty is relatively high, and it is difficult to determine whether sedimentation rates were constant during deposition.

The eastern basin has a mostly flat (mean depth  $\approx$ 10 m) harbor floor that rises along a 3.5–4° gradient toward the shoreline in the north, south, and east (Figure 2). In the eastern basin, we resolved continuous reflections up to 15 m below the harbor floor (Figure 4b). Seismic-reflection profiles reveal an irregular basement (i.e., the top of the lowermost resolvable layer), four main seismic horizons between the basement and harbor floor (referred to as H1–H4 in Figure 4), a wedge-shaped group of chaotic reflections in the shallow subsurface, seafloor valleys that crosscut sea mounds, and erosional unconformities at the base of two prograding clinoforms referred to as clinoform groups 1 and 2 (Figures 4 and 5).

Cores from the northeastern basin slope (see cores J8 and J9 in Figure 3) contain  $\sim$ 22 cm of mostly black unstratified muds that are overlain by 2–6 cm of either brown sands or gray-black silts. The black muds are underlain by alternating  $\sim$ 0.25–0.5 cm thick beds of black, brown, and gray sands, clays, and silts. Some beds are conformably stratified, whereas others are deformed (i.e., tilted with apparent dips of 9–12°, offset or have wavy, convolute, and fluidized internal structures). Excess Pb-210 in one core (i.e., J8) increases stepwise from 4.28–6.16 to 7.58–8.15 dpg/m at 0–10 cm and 15–22 cm below the top of the core, respectively (Figure 3). This decay profile is common for sediments that have undergone mixing/reworking such that older, less enriched xs-Pb 210 sediments have been transported to the top of the core (see McHugh et al., 2016, for example). Accordingly, sedimentation rates cannot be directly estimated from core J8's excess Pb-210 decay profile.

##### 4.1. Basement Geometry and Age Analysis

Three-dimensional interpolation of the basement reflections (Figure 5) shows that the top of the basement shallows eastward (from 9 to 20 mbsl). The geometry of the top of the basement creates a bow-shaped valley that borders two triangular platforms (elevation = 18–22 mbsl) with relatively steep margins (Figures 4b and 5). The floor of the bow-shaped valley is undulatory in some sections and more evenly sloping in others (Figures 4 and 5). The bow-shaped valley floor also hosts a series of raised or elevated structures/blocks (Figures 4b, 4c, and 5).

We suggest that the basement likely represents late Pleistocene-aged Liguanea fan gravel because it is within 0–2 m of the top of the interpreted gravel on the tombolo (see Figure 2b). The basement's undulatory surface (Figures 4b and 4c) also indicates that it is, like the top of the Liguanea fan gravels, an erosive surface (Figure 2b; Goreau & Burke, 1966).

##### 4.2. Seismic Horizon Geometry and Age Analysis

The four main seismic horizons (Figures 4a, 4b, and 5) and two erosional unconformities (Figure 4a) provide information for relative sediment ages and the continuity of sediment deposition in the Harbor. Horizons 1–4 generally have subhorizontal apparent dips (average = 0.1°), terminate against the basement (including the margins of the triangular platforms), lack significant undulation, and deepen southeastward (Figure 5). The horizons are not continuously traceable across the entire Harbor (Figure 5); however, this may be attributed to changes in sedimentary properties. For example, relatively poorer seismic penetration in the western basin could be related to its larger grain sizes, which typically leads to greater attenuation of CHIRP seismic signals (e.g., Lee et al., 2008; Pinson et al., 2008; Vardy, 2015). Furthermore, we have chosen not to interpret

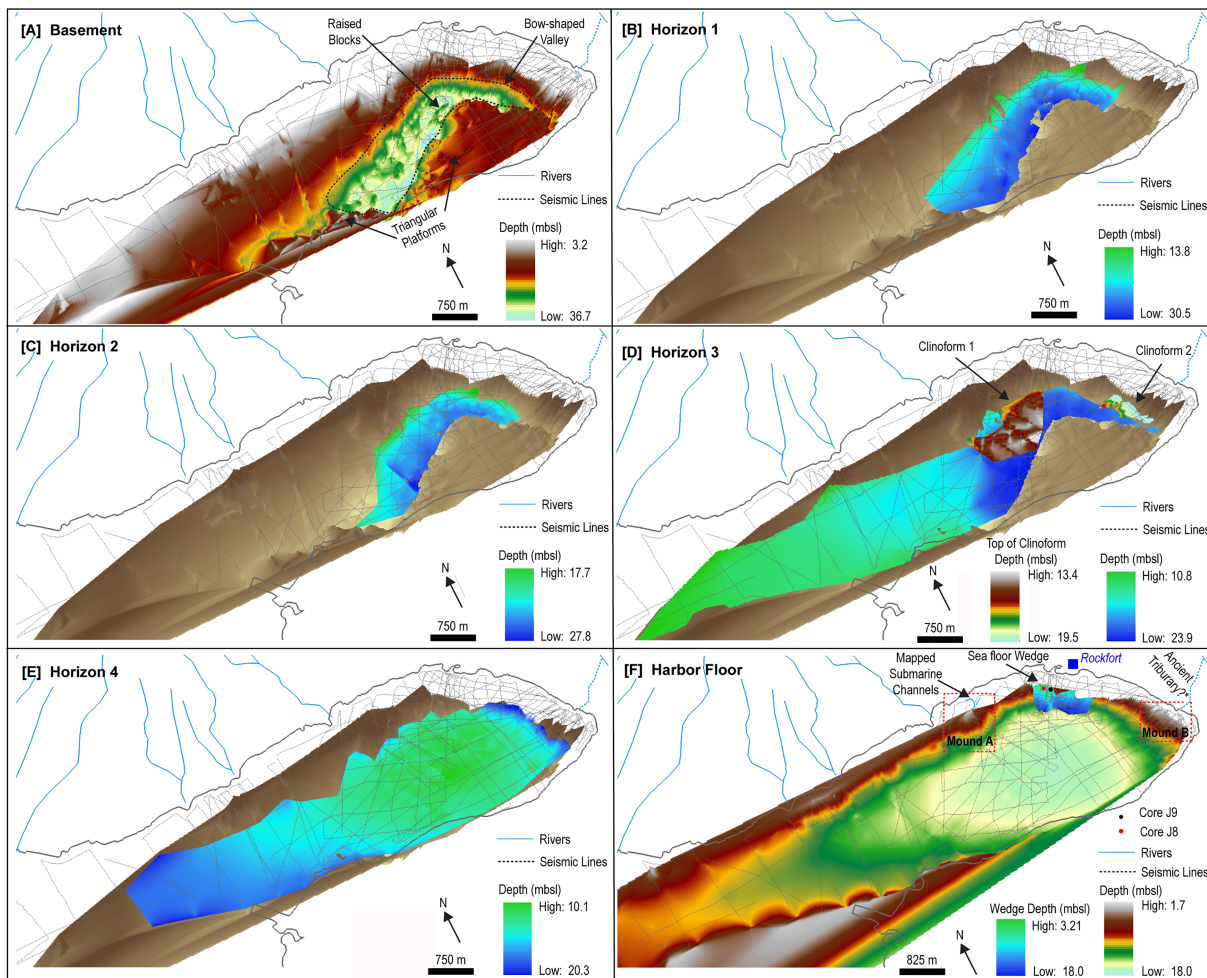


**Figure 5.** Diagram showing a 2.5-dimensional oblique view of the horizons and the areal extents of the seafloor wedge, the clinoforms (interpreted from prograding reflectors), and seafloor mounds in the Harbor. The brown image beneath horizons 1–4 is the basement. Zoomed in images of the basement raised blocks (Figure 5a), clinoforms (Figure 5d), and the seafloor wedge (Figure 5f) can be found in the supporting information. An example seismic-reflection profile showing clinoform group 1 is shown in Figure 4b (Line 4B), and an example seismic-reflection profile showing clinoform group 2 is shown in the supporting information.

the lack of continuity of the horizons as products of erosion because we have only identified two main erosional unconformities within the Harbor. The erosional unconformities are between horizons 2 and 3 (Figure 4a). One is between 17.4 and 21 mbsl and restricted to the northeastern section of the eastern basin (below prograding clinoforms—see Figures 4b and 5) where it spans an area of 147,883 m<sup>2</sup>. The second is between 18 and 21 mbsl and restricted to the easternmost section of the eastern basin, where it spans an area of 940,362m<sup>2</sup>. Together, these observations indicate that sediments imaged in the Harbor were likely deposited between the latest Pleistocene to present without significant episodes of basin-wide erosion. Most of the analysis will, therefore, focus on the eastern basin, where seismic penetration is better.

### 4.3. Seafloor Sediment Wedge Geometry and Age Analysis

The seafloor wedge is imaged on the northeastern slope, where it is overlain by ~1–2 cm of sediments (Figures 4c, 5, and 7e). The wedge's internal reflectivity is generally acoustically incoherent (chaotic) or wavy (Figure 4c). The wedge thickens shoreward to 9.28 m. Its area and volume are 290,000 m<sup>2</sup> and 762,000 ± 21,000 km<sup>3</sup>, respectively (Figures 4c and 5). Cores J8 and J9's (Figure 3) direct sampling of the top 100 cm of 4 m thick sections of the wedge (Figure 5), along with its continuous yet wavy internal reflections, suggest that the sediments are likely a mix of sands or finer-grained sediments.

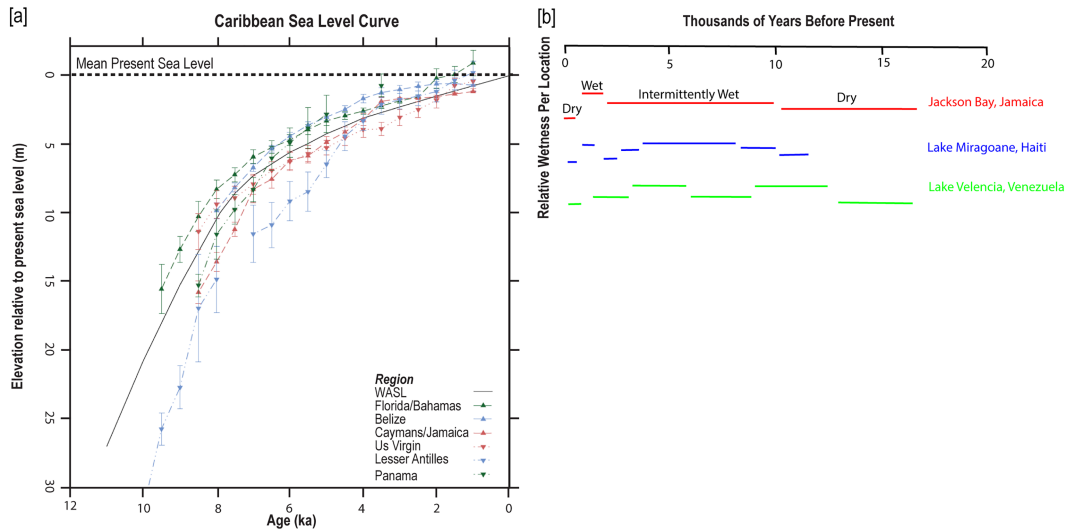


**Figure 6.** (a) Graph shows the Caribbean-wide relative sea level curves adapted from Jackson (2013). The abbreviation WASL refers to the Western Atlantic sea level. (b) Graph adapted from McFarlane et al. (2002) shows interpretations for the relative wetness (precipitation intensities) based on geochemical analyses of sediments and or fossils in Jackson Bay Jamaica, Lake Miragoane Haiti, and Lake Valencia Venezuela.

The seafloor wedge was likely deposited by a mass flow event. Support for this interpretation comes from (1) other seismic and coring studies that have confidently associated mass flow deposits with chaotic reflectivity (e.g., McHugh et al., 2011; McHugh et al., 2014; Moernaut et al., 2009) and (2) the sediments in cores J8–J9, which we interpreted (based on its Pb-210 profile) to have either been mixed, reworked, or deformed. Furthermore, we interpret that a mass flow event could lead to the inverted xs-Pb210 profile observed in core J8. Here, less enriched xs-Pb-210 would exist at the top of the core if the sediments skimmed the top of the seafloor during the mass flow event.

Potential causes for the interpreted mass flow deposits include strong ground shaking during an earthquake, hurricanes/intense rainfall that destabilize the Harbor slopes, or anthropogenic sediment dumping. Here, we prefer the earthquake-induced submarine failures interpretation because (1) both the 1692 and 1907 Jamaican earthquakes have caused beach floor submergence and soft-sediment flowage within the Harbor (Sloane, 2009; Fuller, 1907), (2) there are no known reports of any businesses or government agencies dumping  $762,000 \pm 21,000 \text{ km}^3$  of sediments within this or any section of the Harbor, and (3) while Hurricanes have caused seiches that could disturb sediments, there are no known reports of hurricane or intense rainfall events that have triggered mass wasting deposits within the Harbor. The deformation observed in the cores (i.e., tilted and fracture beds, convolute structures, and fluidized sediments) are also more common with mass flow event and/or earthquake shaking as opposed to earthquakes or anthropogenic dumping (e.g., McHugh et al., 2011; McHugh et al., 2014). Here, we recognize that sediment deformation could also occur due to disturbance during coring; however, the presence of seismic and xs-Pb 210 evidence for mass flow sediment deposition leads us to interpret that these core-observed sediment deformation features are also likely natural.

Compared to the 1692 earthquake, we propose that the ground shaking during the 1907 earthquake is the more likely cause of the mass flow deposits. Reports from the 1907 earthquake are the only ones revealing that Rockfort (the community adjacent to the mass flow deposits) was a site of extensive sediment deformation that likely extended onshore (Sloane, 2009; Fuller, 1907). Both pictures and written descriptions show that Rockfort's coastal region experienced liquefaction that caused the tilting of the land and trees toward the Harbor, coastal subsidence, and lateral spreads (Fuller, 1907). Based on the interpretation that the 1907 event caused the mass wasting deposits in the Harbor, we estimate that sedimentation rates along the northeast slope of the Harbor were between 0.024 and 0.057 cm/year for the last 106 years.

#### 4.4. Clinoform, Mount, and Depressions Geometry and Age Analysis

Clinoform groups 1 and 2 are represented by wedge-shaped groups of low-angle oblique reflections respectively mapped on the northeastern and eastern basin slopes within the eastern basin (Figure 5). The tops of

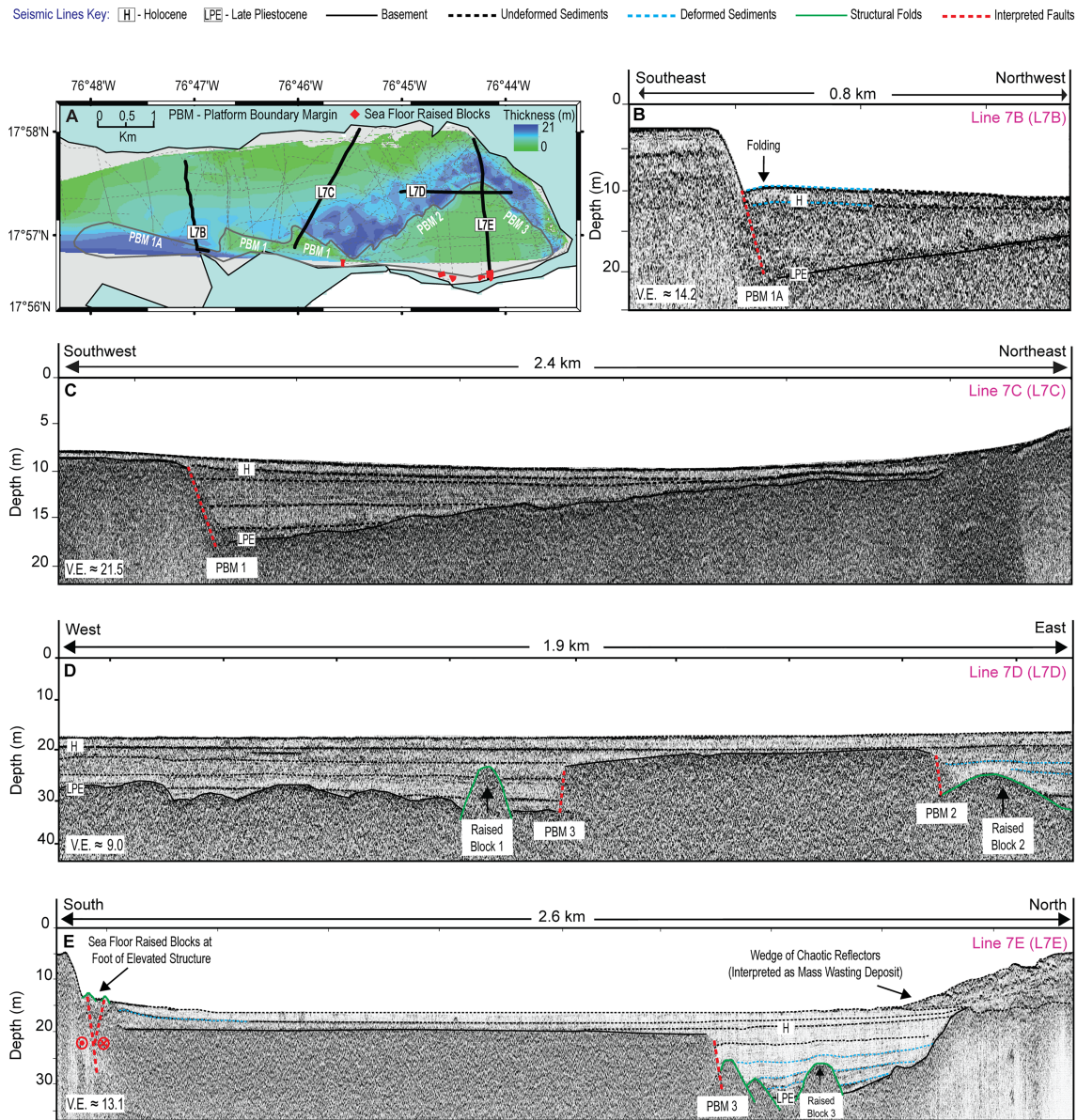


**Figure 7.** (a) Map shows a total sediment thickness between the harbor floor and basement, track lines seismic profiles collected across the harbor (dashed gray lines), and the outline of the triangular platform (thick grey solid line). The seismic profiles for seismic track lines L7B-L7E are shown in Figures 7b–7e, respectively. Figures 7a–7c show that up to three seismically distinguishable sedimentary units terminate against or continue above platform boundary margin 1. Figures 7a and 7d show that three to four seismically distinguishable units terminate against platform boundary margins 2–3, and 1–2 units continue above them. We interpret that the three platform boundary margins are fault bounded. These are later referred to as faults 1–3.

the clinoforms thin seaward (13–19 mbsl), and their bases are represented by subhorizontal erosional unconformities located between 18 and 21 mbsl.

Both clinoforms line the foot of or extend away from a sea mound (Figures 4b and 5). The mound adjacent to clinoform group 1 (named mound A) is crosscut by two rectangular-shaped (in profile view) valleys (Figure 4d). This mound is 240–590 m west of a present-day onshore river (Figure 5). The mound adjacent to clinoform group 2's (named mound B) is within a few meters of the mouths of abandoned (within the last 400 years) tributaries of the Hope River (Figure 5). We did not identify a valley that down cuts into this mound.

We interpret that the valleys and mounds are fluviodeltaic systems and that they likely deposited the clinoforms because (1) the mounds and valleys are within 10–590 m from mouths of present-day or ancient

drainages and (2) the two rectangular-shaped (in profile view) valleys (Figure 4d) that crosscuts Mound A likely represent a floodplain with a smaller meandering channel (Figure 5). We also suggest that the sediment drainages most likely deposited clinoforms because the clinoforms thin and prograde seaward (indicating a landward source) and are only identifiable downdip from the valleys—that is, at the foot of delta lobes in the eastern basin. Here, the observation that both clinoforms have subhorizontal bases at an average depth of ~19 mbsl indicates that both clinoforms were likely deposited at the same time and possibly by similar processes.

We use sequence stratigraphic analyses and sea level curves from the Caribbean (Digerfeldt & Hendry, 1987; Jackson, 2013; Figure 6) and the world (Bianchi et al., 2012) to determine the timing of and processes leading to clinoform deposition. The clinoforms could have been deposited during either a transgression or a regression. Here, we interpret that the clinoforms were deposited during a transgression because clinoforms would not have been preserved if they were deposited during the last global or regional regression (i.e., during the last interglacial period (120–20 k.a.) when sea levels fell from ~9–120 mbsl). We also found no evidence of harbor-wide tectonic uplift that could have induced a local regression in the Harbor, making clinoform deposition during transgression more likely.

For clinoforms to develop during a transgression, sedimentation rates need to be faster than the rate at which sea level changes create accommodation space (Posamentier & Morris, 2000; Vail & Mitchum, 1977). For Jamaica, this condition would have been best achieved between 10 and 8 k.a. when sedimentation rates were likely high due to significant uptakes in precipitation, heat, and erosion (see Hodell et al., 1991; Martin et al., 1997; McFarlane et al., 2002, for examples). In shallow marine environments offshore Haiti (e.g., Rios et al., 2013), sediments deposited under the Holocene sea level and paleoclimate conditions create a thick and uniform zone of acoustic transparency in high-resolution chirp seismic data. This is similar to what we observe above the clinoforms in the Harbor (Figure 4b). Furthermore, assuming a constant sedimentation rate within this section of the Harbor (i.e., 0.024–0.057 cm/year) reveals that the maximum age for the base of the clinoforms is 10.4 k.a. The above sea level, paleoclimate, sedimentation rate, and seismic reflectivity analyses, therefore, suggest that clinoforms began to develop at the start of the Holocene.

## 5. Tectonic Deformation Within Kingston Harbor

The above stratigraphic analysis indicates that the age of the top-of-basement surface and horizon 2 is latest Pleistocene and Holocene, respectively. The analysis also suggests that Holocene sedimentation rates (derived from geochemical studies of cores and seismic stratigraphy) are between 0.05 and 0.20 cm/year. Here, we use the age-dating results and sediment thickness (determined from the seismic horizons), dip, offset, and terminations to identify faults, assess their relative motion, and estimate their timing of movement. Our analyses focus on determining whether the linear boundary margins of the triangular platforms (henceforth referred to as platform boundary margins 1–3) and elevated blocks within the basement and seafloor (see Figure 7) are associated with active tectonics in eastern Jamaica.

### 5.1. Sediment Deformation Analysis

Platform boundary margin 1's (PBM1's) mean strike and total lengths are N53°W and 4.1 km, respectively (Figure 7a). The thickness of the shallowest unit adjacent to the northwesternmost 1.5 km of the platform boundary (referred to as platform boundary 1A) is 1.4–1.8 m for the first 200–600 m from the north but thickens and folds (concave upward) within the last 505 m of the platform boundary prior to terminating via onlap onto the boundary margin (Figure 7b). The lower unit adjacent to platform boundary 1A both thickens toward the platform and southeasterly along strike of the platform. The unit tilts toward the platform boundary margin with an apparent dip between 0.1° and 0.3°. East of platform boundary margin 1A, all units (except for the shallowest unit) thicken and slightly tilt (apparent dips = 0.1–0.7°) toward the platform boundary margin (Figures 7a and 7c).

Platform boundary margin 2 (PBM2) is 6 km long, and its mean strike is N50E (Figure 7a). The thickness of the shallowest unit adjacent to the platform boundary margin remains constant (1.4–1.8 m) toward the platform boundary margin (Figure 7d). The unit's mean apparent dip is 0.01°. All deeper units (i.e., units 2–5) show some degree of thickening but only very slight tilting (i.e., 0.01° and 0.20° apparent dips) toward

platform boundary margin 2 (Figures 7a and 7d). The units also exhibit varying degrees of thickening along strike of the platform boundary.

Platform boundary margin 3 (PBM3) is 2 km long, and its mean strike is N45 W (Figure 7a). The northern 0.2 km of this platform boundary margin is bordered by one to two 5–7 m high elevated blocks (e.g., Figures 7a, 7d, and 7e). All units adjacent to these structures either thicken and progressively increase their dips toward the fold surfaces (e.g., Figure 7e) or slightly fold above it (e.g., Figure 7d). Except for the shallowest unit (which maintains its thickness), all units above and south of the fold structures thicken but do not significantly tilt with depth.

Along with the linear platform boundary margins, we also observed and assessed at least three other structures for possible evidence of tectonic deformation. They include the elevated blocks within the bow-shaped valley, the tilting of the easternmost triangular platform, and the elevated block within the seafloor located directly above the easternmost platform (Figure 7).

The elevated blocks within the bow-shaped valley trend in a N78°W direction between platforms 1 and 2 (see trends in Figure 7a, and see elevated blocks in Figures 7d and 7e). Sediments generally (e.g., see Figures 4b, 7d, and 7e) thicken, progressively tilt, and rotate toward the blocks. Sediments also sometimes thin within the last 50 m before terminating via onlap (e.g., see Figures 4b, 7d, and 7e). Sediments above some of the blocks are slightly folded (Figure 7e).

The larger triangular platform tilts (mean apparent dip = 0.1°) toward the southwest, and sediments above it thicken to the southwest (Figures 7a, 7d, and 7e). Sediments terminate against a 5–7 m high (relative to the platform surface) structure that trends east southwest for at least 3.2 km along the southernmost edge of the platform (e.g., Figures 7a and 7e). The seafloor directly adjacent to the foot of this structure hosts a disconnected group of 0.75–1.5 m raised blocks (e.g., Figure 7e) that trends for 3 km parallel (W-E) to the 5–7 m high structure (see Figure 7a for trends).

## 5.2. Sediment Deformation Interpretations

Of the three platform boundaries, we only observed deformed sediments adjacent to the northwestern sections of platform boundary margins 3 and 1 (Figures 7b, 7d, and 7e). Here, we interpret the northwest 0.9 km of platform boundary margin 3 as a fault because the adjacent Pleistocene-aged deposits show evidence for syntectonic deformation (i.e., sediments are progressively steeper with depth and thicken toward the platform boundary margin (Figure 7e)). We also interpret platform boundary margin 1A (Figure 7b) as a fault because the adjacent sediment deformation (i.e., concave folding before termination via onlap) is similar to drag folds that develop due to upthrown motion along a fault's hanging wall. It could also occur due to extensional tectonism along a listric fault, but we tentatively rule this interpretation out because the imaged sections of platform boundary margin 1A appear planar. We did not find clear evidence for similar syntectonic sediment deformation along other sections of both platform boundary margins (Figure 7c). These observations imply that the faults bounding platforms 3 and 1 may have different rupture histories.

Syntectonic deformation was also not found along platform boundary margin 2 as sediments thickened along strike but show no progressive tilting with depth (Figure 7d). Since the platform boundary margin is located between two faults and its strike is the only one (of the three platform boundary margins in the Harbor) favorably oriented for extension under Jamaica's mid-Miocene to present sinistral stress regime, we infer that platform boundary margin 2 may represent a normal or dip slip fault that has been relatively inactive or has had mostly fault parallel motion since at least the late Pleistocene. Given that the analyses suggest that all the platforms are bound by faults, we will henceforth refer to platform boundary margins 1–3 as faults 1–3.

The elevated blocks in the bow-shaped valley (Figures 7a and 7d) could be interpreted as the bathymetric expressions of blind faults, carbonate reefs, or leftover sediment buildups after erosion or deposition. Here, features indicating the possibility of blind faulting include the blocks' segmented nature, their relatively narrow cross-sectional widths (<100 m), and their linear trend (N78°W) that points toward elongation often observed in buried strike-slip faults (Wu et al., 2009). Other features indicating the possibility of blind faulting include sediments folding above some blocks and thickening and dipping of the sediments toward the blocks (e.g., Mann et al., 1983; Wu et al., 2009). One alternative hypothesis is that the sediment deformation observed (particularly folding directly above the blocks) could also be due to sediment compaction as

opposed to tectonic activity. A second alternative hypothesis is that the blocks are leftover carbonate reef or gravel sediments caused by erosion of an ancient river—perhaps the Hope River. This alternative hypothesis would imply that the Hope river once flowed in an east-west direction, which is opposite to the general north-south trend of all other streams within this region. Given that the sediment deformation associated with the raised blocks could be the result of multiple geologic processes, more studies (with deeper penetrating seismic lines) are required to provide a confident interpretation of these features.

We interpret that an active fault zone deforms the triangular platform (i.e., faults 2–3's footwall). The south-westward tilting of faults 2–3 footwall that coincides with sediment thickening may be explained by active faulting along the 3 km-long elevated structure adjacent to the seafloor raised blocks (Figure 7e). Furthermore, we suggest that this is an oblique-slip fault zone because disconnected pairs of seafloor folds (especially those extending linearly for over 3,000 m) are common expressions of buried flower structures (e.g., Corbeau et al., 2016; Mann et al., 1983; Wu et al., 2009). Scree or mass wasting deposits triggered by either the 1692 or 1907 earthquake is one possible explanation for the raised blocks on the seafloor, but this ignores the sediment deformation adjacent to the blocks, and we have no other data to support this alternative interpretation.

## 6. Discussion

### 6.1. Strain Accommodation With the Fault System

Overall, our sediment deformation analyses indicate that the Harbor hosts at least three faults (faults 1–3) that created a Pleistocene or older-aged basin. This basin is currently being deformed by a strike-slip fault along the southern boundary of the Harbor. Fault 3 is the only one that has deformed late Pleistocene sediments, whereas both fault 1 and the strike-slip fault on the southern border of the Harbor are the only ones that have deformed Holocene sediments.

Vertical upward motion of the hanging wall of fault 1A (previously referred to as platform boundary margin 1A), alongside tilting of the footwalls of faults 2 and 3 likely occurred after the development of the basin created by active slippage along faults 1–3. Here, we interpret that fault 1A extends eastwardly across the Harbor, where it connects with the interpreted fault that crosscuts faults 1–2's footwall. Both faults (i.e., fault 1A and the crosscutting footwall fault) may be part of a larger oblique-slip fault system, which, consistent with other studies, increases or decreases its displacement and method of strain accommodation based on its strike and local crustal structures (e.g., Mann et al., 1983; Seeber et al., 2006). Scissoring downward (toward the west) motion followed (or accompanied) by uplift along this fault could, therefore, explain not only why fault 1A is the only fault with adjacent compressional sediment deformation within the Harbor but also the tilting of the footwall of faults 2 and 3.

### 6.2. Relationship Between Onshore and Offshore Faults

Fault 1A is the only fault that likely connects to a known onshore fault system (i.e., the Bull Bay Strike-Slip Fault; Figure 1). Fault 2 is terminated by both faults 1 and 3 and is therefore unlikely to be connected to any known onshore faults. Both fault 3's southeastward and northwestward projections align with thrust faults. Because fault 3 is either a normal or dip-slip fault, we interpret that fault 2 is unlikely to be an extension of these thrust faults (Figure 1). We previously interpreted that fault 1A is an extension of the interpreted strike-slip fault that trends east-west within the hanging walls of faults 2 and 3. Here, we also interpret that these Harbor faults represent an extension of the Bull Bay Fault because both are oblique-slip or strike-slip systems, and they have roughly the same strikes (Figure 1).

Identification of the extension of the Bull Bay Fault is important for seismic hazard assessment within southeastern Jamaica. Empirical relationships between fault length and magnitude (Wells & Coppersmith, 1994) indicate that a complete rupture of this fault (interpreted to be ~22 km long when harbor faults are included) could generate  $M_w$  6.2–6.9 earthquake. Half the length of this fault may generate a  $M_w$  5.8–6.5 earthquake. A  $M_w$  5.8–6.9 event along the fault system could cause an unexpected level of damage because (1) Jamaica's seismic hazard maps only account for 5.8–6.9  $M_w$  earthquakes on faults east of the Wagwater Belt and (2) the faults trend within sedimentary basins, which amplify seismic waves by factors of 3–10 (Wiggins-Grandison, 2001; Salazar et al., 2013).

When the newly identified fault systems are analyzed in the context of the EPGFZ flower structure, our analyses imply that Kingston Harbor is perhaps a microcosm for the rest of Southeastern Jamaica. Strain accommodation within the EPGFZ in eastern Jamaica appears to take one of two main forms—that is, fault structure interactions either leads to (1) inversion of preexisting normal faults or (2) extension and subsidence prior to inversion and deformation via uplift, folding, or shortening (James-Williamson et al., 2014; Mann et al., 1985; Mann et al., 2007). The style of deformation within the harbor fault system is consistent with (2) above as we show that motion along faults 1–3 creates a pre-Pleistocene age basin that is currently being deformed by the Bull Bay Strike-Slip Fault. Our analyses also show that the boundary of the EPGFZ, which was once thought to end at the LMFS, is likely broader and perhaps more hazardous than previous studies recognized.

## 7. Conclusions

Offshore Kingston Harbor Jamaica hosts sedimentary facies dating from at least the latest Pleistocene to present. These facies include the Liguanea fan gravels, latest Pleistocene to present terrigenous sands, prograding clinoforms, submarine slide deposits potentially triggered by earthquakes, and submerged fluviodeltaic systems. In the eastern basin, the base of the Holocene is marked by clinoforms that likely developed due to increased drainage associated with an increase in precipitation and erosion. Current (Holocene-aged) tectonic deformation is localized along the southern edge of the Harbor, where strain is accommodated via structural folding and oblique-slip motion.

The Harbor faults are a smaller part of a ~22 km-long sinistral fault system that could generate a  $M_w$  5.8–6.9 earthquake. This fault system (i.e., Bull Bay Strike-Slip Fault) is one of the boundary faults for a flower structure that has been expanding southwestward across eastern Jamaica since the mid-Miocene. Its extension into the Harbor provides the first evidence that the EPGFZ flower structure extends into Kingston, the capital city where two thirds of the population live.

Our interpretations may be further tested by acquiring deeper penetrating seismic data and sediment cores within Harbor, the Liguanea Fan, and the South Coast of Jamaica. Such images and cores may also allow future studies to improve the age-dating model presented in this paper, examine the relationship between faults 1–3, and assess deformation rates in greater detail. Data from the surveys may provide paleoseismic information that can be used to improve understanding of transpression, fault segmentation, accommodation, earthquake rupture nucleation, and earthquake recurrence intervals.

### Acknowledgments

This work was supported by the National Science Foundation under Grant EAR-1042906 to UNAVCO and the Society of Exploration Geophysicists (SEG) “Geophysicists without Borders.” We thank Carris G., Flynn C., Frone Z., Fontana J., Giddens E., Klauser A., Mattingly B., Mauroner C., Phrampus B., the Jamaica Defense Force, and the Jamaican Coast Guard for their contributions during our field surveys. We also thank Magnani M. for constructive feedback during manuscript preparation, Bopp R. for performing the gamma ray bombardment analysis of sediments, and Gulseth C. for providing sediment cores J10–J11. We also thank the reviewers for constructive feedback during formal manuscript revisions, especially Koehler R., for two rounds of detailed reviews. This research used the IHS Kingdom Suite software, which is donated to SMU through their educational program. The seismic profiles used in this study are archived at the Academic Seismic Portal at University of Texas Institute of Geophysics (DOI:10.1594/IEDA/500256).

### References

- Abbott, R. N. Jr., West, D. P., Bandy, B. R., & McAleer, R. J. (2016). Petrology and tectonic history of the Green Bay Schist, Portmore, St. Catherine Parish, Jamaica. *Caribbean Journal of Earth Sciences*, 48, 1–18.
- Andrews, J. E., Greenaway, A. M., & Dennis, P. F. (1998). Combined carbon isotope and C/N ratios as indicators of source and fate of organic matter in a poorly flushed, tropical estuary: Hunts Bay, Kingston Harbour, Jamaica. *Estuarine, Coastal and Shelf Science*, 46(5), 743–756. <https://doi.org/10.1006/ecss.1997.0305>
- Bakun, W. H., Flores, C. H., & ten Brink, U. S. (2012). Significant earthquakes on the Enriquillo fault system, Hispaniola, 1500–2010: Implications for seismic hazard. *Bulletin of the Seismological Society of America*, 102(1), 18–30. <https://doi.org/10.1785/0120110077>
- Benford, B., DeMets, C., Tikoff, B., Williams, P., Brown, L., & Wiggins-Grandison, M. (2012). Seismic hazard along the southern boundary of the Gonaive microplate: Block modelling of GPS velocities from Jamaica and nearby islands, northern Caribbean. *Geophysical Journal International*, 190(1), 59–74. <https://doi.org/10.1111/j.1365-246x.2012.05493.x>
- Bianchi, C. N., Morri, C., Chiantore, M., Montefalcone, M., Parravicini, V., & Rovere, A. (2012). Mediterranean Sea biodiversity between the legacy from the past and a future of change. In *Life in the Mediterranean Sea: a look at habitat changes* (pp. 1–55). New York: Nova Science Publishers, Inc.
- Burke, K. (1967). The Yallahs Basin: A sedimentary basin southeast of Kingston, Jamaica. *Marine Geology*, 5(1), 45–60.
- Cochran, W. J., Spotila, J. A., Prince, P. S., & McAleer, R. J. (2017). Rapid exhumation of Cretaceous arc-rocks along the Blue Mountains restraining bend of the Enriquillo-Plantain Garden fault, Jamaica, using thermochronometry from multiple closure systems. *Tectonophysics*, 721, 292–309. <https://doi.org/10.1016/j.tecto.2017.09.021>
- Corbeau, J., Rolandone, F., Leroy, S., De Lepinay, B. M., Meyer, B., Ellouz-Zimmermann, N., & Momplaisir, R. (2016). The northern Caribbean plate boundary in the Jamaica Passage: Structure and seismic stratigraphy. *Tectonophysics*, 675, 209–226. <https://doi.org/10.1016/j.tecto.2016.03.022>
- DeMets, C., & Wiggins-Grandison, M. (2007). Deformation of Jamaica and motion of the Gonaive microplate from GPS and seismic data. *Geophysical Journal International*, 168(1), 362–378. <https://doi.org/10.1111/j.1365-246x.2006.03236.x>
- Digerfeldt, G., & Hendry, M. D. (1987). An 8000 year Holocene sea-level record from Jamaica: Implications for interpretation of Caribbean reef and coastal history. *Coral Reefs*, 5(4), 165–169. <https://doi.org/10.1007/bf00300959>
- Draper, G. (2008). Some speculations on the Paleogene and Neogene tectonics of Jamaica. *Geological Journal*, 43(5), 563–572. <https://doi.org/10.1002/gj.1124>
- Fuller, M. L. (1907). Notes on the Jamaica earthquake. *The Journal of Geology*, 15(7), 696–721. <https://doi.org/10.1086/621461>

- Goodbody, I. (2003). Kingston Harbour, Jamaica—An overview. *Bulletin of Marine Science*, 73(2), 249–256.
- Goreau, T., & Burke, K. (1966). Pleistocene and Holocene geology of the island shelf near Kingston, Jamaica. *Marine Geology*, 4(3), 207–224. [https://doi.org/10.1016/0025-3227\(66\)90021-1](https://doi.org/10.1016/0025-3227(66)90021-1)
- Hayes, G. P., Briggs, R. W., Sladen, A., Fielding, E. J., Prentice, C., Hudnut, K., et al. (2010). Complex rupture during the 12 January 2010 Haiti earthquake. *Nature Geoscience*, 3(11), 800–805. <https://doi.org/10.1038/ngeo977>
- Henkart, P. (2006). Chirp sub-bottom profiler processing—A review. *Sea Technology*, 47(10), 35–38.
- Hodell, D. A., Curtis, J. H., Jones, G. A., Higuera-Gundy, A., Brenner, M., Binford, M. W., & Dorsey, K. T. (1991). Reconstruction of Caribbean climate change over the past 10,500 years. *Nature*, 352(6338), 790. <https://doi.org/10.1038/352790a0>
- Hornbach, M. J., Mann, P., Frohlich, C., Ellins, K., & Brown, L. (2011). Assessing geohazards near Kingston, Jamaica: Initial results from chirp profiling. *The Leading Edge*, 30(4), 410–413. <https://doi.org/10.1190/1.3575287>
- Horsfield, W. (1974). Major faults in Jamaica. *Journal of the Geological Society of Jamaica*, 14, 1–15.
- Jackson, L. P. (2013). Caribbean sea level change: Observational analysis from millennial to decadal timescales, (Doctoral dissertation). Retrieved from White Rose eTheses Online. (<http://etheses.whiterose.ac.uk/5779/>). Leeds, West Yorkshire: University of Leeds.
- James-Williamson, S. A., Mitchell, S. F., & Ramsook, R. (2014). Tectono-stratigraphic development of the Coastal Group of south-eastern Jamaica. *Journal of South American Earth Sciences*, 50, 40–47. <https://doi.org/10.1016/j.jsames.2013.11.005>
- Koehler, R. D., Mann, P., Prentice, C. S., Brown, L., Benford, B., & Wiggins-Grandison, M. (2013). Enriquillo–Plantain Garden fault zone in Jamaica: Paleoseismology and seismic hazard. *Bulletin of the Seismological Society of America*, 103(2A), 971–983. <https://doi.org/10.1785/0120120215>
- Lee, G. H., Kim, H. J., Kim, D. C., Yi, B. Y., Nam, S. M., Khim, B. K., & Lim, M. S. (2008). The acoustic diversity of the seabed based on the similarity index computed from Chirp seismic data. *ICES Journal of Marine Science*, 66(2), 227–236. <https://doi.org/10.1093/icesjms/fsn142>
- Mann, P., DeMets, C., & Wiggins-Grandison, M. (2007). Toward a better understanding of the Late Neogene strike-slip restraining bend in Jamaica: Geodetic, geological, and seismic constraints. *Geological Society, London, Special Publications*, 290(1), 239–253. <https://doi.org/10.1144/sp290.8>
- Mann, P., Draper, G., & Burke, K. (1985). Neotectonics of a strike-slip restraining bend system, Jamaica. In K. T. Briddle, & N. Christie-Blick (Eds.), *Strike-Slip Deformation, Basin Formation, and Sedimentation*, (Vol. 37, pp. 211–226). Broken Arrow, OK: SEPM society for sedimentary geology. <https://doi.org/10.2110/pec.85.37.0211>
- Mann, P., Hempton, M. R., Bradley, D. C., & Burke, K. (1983). Development of pull-apart basins. *The Journal of Geology*, 91(5), 529–554.
- Martin, L., Bertaux, J., Corrège, T., Ledru, M. P., Mourguiart, P., Sifeddine, A., et al. (1997). Astronomical forcing of contrasting rainfall changes in tropical South America between 12,400 and 8800 cal yr BP. *Quaternary Research*, 47(1), 117–122. <https://doi.org/10.1006/qres.1996.1866>
- McFarlane, D. A., Lundberg, J., & Fincham, A. G. (2002). A late Quaternary paleoecological record from caves of southern Jamaica, West Indies. *Journal of Cave and Karst Studies*, 64(2), 117–125.
- McHugh, C. M., Kanamatsu, T., Seeber, L., Bopp, R., Cormier, M. H., & Usami, K. (2016). Remobilization of surficial slope sediment triggered by the AD 2011 Mw 9 Tohoku-Oki earthquake and tsunami along the Japan Trench. *Geology*, 44(5), 391–394. <https://doi.org/10.1130/G37650.1>
- McHugh, C. M., Seeber, L., Braudy, N., Cormier, M. H., Davis, M. B., Diebold, J. B., et al. (2011). Offshore sedimentary effects of the 12 January 2010 Haiti earthquake. *Geology*, 39(8), 723–726. <https://doi.org/10.1130/g31815.1>
- McHugh, C. M., Seeber, L., Cormier, M. H., & Hornbach, M. (2014). Submarine paleoseismology along populated transform boundaries: The Enriquillo–Plantain–Garden Fault, Canal du Sud, Haiti, and the North Anatolian Fault, Marmara Sea, Turkey. *Oceanography*, 27(2), 118–131. <https://doi.org/10.5670/oceanog.2014.47>
- Moernaut, J., De Batist, M., Heirman, K., Van Daele, M., Pino, M., Brümmer, R., & Urrutia, R. (2009). Fluidization of buried mass-wasting deposits in lake sediments and its relevance for paleoseismology: Results from a reflection seismic study of lakes Villarrica and Calafquén (South-Central Chile). *Sedimentary Geology*, 213(3–4), 121–135. <https://doi.org/10.1016/j.sedgeo.2008.12.002>
- Pinson, L. J., Henstock, T. J., Dix, J. K., & Bull, J. M. (2008). Estimating quality factor and mean grain size of sediments from high-resolution marine seismic data. *Geophysics*, 73(4), G19–G28. <https://doi.org/10.1190/1.2937171>
- Posamentier, H. W., & Morris, W. R. (2000). Aspects of the stratal architecture of forced regressive deposits. *Geological Society, London, Special Publications*, 172(1), 19–46. <https://doi.org/10.1144/gsl.sp.2000.172.01.02>
- Rios, J., McHugh, C., Hornbach, M., Mann, P., Wright, V., & Gurung, D. (2013). Holocene activity of the Enriquillo–Plantain Garden Fault in Lake Enriquillo derived from seismic stratigraphy. *AGU Fall Meeting Abstracts*, 1, 2629.
- Rosencrantz, E., & Mann, P. (1991). SeaMARC II mapping of transform faults in the Cayman Trough, Caribbean Sea. *Geology*, 19(7), 690–693. [https://doi.org/10.1130/0091-7613\(1991\)019<0690:SIMOTF>2.3.CO;2](https://doi.org/10.1130/0091-7613(1991)019<0690:SIMOTF>2.3.CO;2)
- Salazar, W., Brown, L., & Mannette, G. (2013). Probabilistic seismic hazard assessment for Jamaica. *Journal of Civil Engineering and Architecture*, 7(9), 1118. <https://doi.org/10.17265/1934-7359/2013.09.007>
- Seeber, L., Cormier, M. H., McHugh, C., Emre, O., Polonia, A., & Sorlien, C. (2006). Rapid subsidence and sedimentation from oblique slip near a bend on the North Anatolian transform fault in the Marmara Sea, Turkey. *Geology*, 34(11), 933–936. <https://doi.org/10.1130/g22520a.1>
- Sloane, H., De Toledo, A., & Morley, C. L. (1694). I. A letter from Hans Sloane, MD and SR S: With several accounts of the earthquakes in Peru October the 20th. 1687. and at Jamaica, February 19th. 1687/8 and June the 7th. 1692. *Philosophical Transactions*, 18(209), 78–100. <https://doi.org/10.1098/rstl.1694.0019>
- Steers, J. A. (1940). The Cays and the Palisadoes, Port Royal, Jamaica. *Geographical Review*, 30(2), 279–296. <https://doi.org/10.2307/210146>
- Vail, P. R., & Mitchum, R. M. (1977). Seismic stratigraphy and global changes of sea level. Part 1: Overview. In C. Payton (Ed.), *Seismic stratigraphy: applications to hydrocarbon exploration*, (Vol. 26, pp. 51–52). Tulsa, OK: American Association of Petroleum Geologists. <https://doi.org/10.1306/M26490C>
- Vardy, M. E. (2015). Deriving shallow-water sediment properties using post-stack acoustic impedance inversion. *Near Surface Geophysics*, 13(2), 143–154. <https://doi.org/10.3997/1873-0604.2014045>
- Wadge, G., & Dixon, T. H. (1984). A geological interpretation of SEASAT-SAR imagery of Jamaica. *The Journal of Geology*, 92(5), 561–581. <https://doi.org/10.1086/628892>
- Wang, J., Mann, P., & Stewart, R. R. (2018). Late Holocene structural style and seismicity of highly transpressional faults in southern Haiti. *Tectonics*, 37, 3834–3852. <https://doi.org/10.1029/2017TC004920>
- Wells, D. L., & Coppersmith, K. J. (1994). New empirical relationships among magnitude, rupture length, rupture width, rupture area, and surface displacement. *Bulletin of the Seismological Society of America*, 84(4), 974–1002.

- Wiggins-Grandison, M. D. (2001). Preliminary results from the new Jamaica seismograph network. *Seismological Research Letters*, 72(5), 525–537. <https://doi.org/10.1785/gssrl.72.5.525>
- Wiggins-Grandison, M. D., & Atakan, K. (2005). Seismotectonics of Jamaica. *Geophysical Journal International*, 160(2), 573–580. <https://doi.org/10.1111/j.1365-246x.2004.02471.x>
- Wu, J. E., McClay, K., Whitehouse, P., & Dooley, T. (2009). 4D analogue modelling of transtensional pull-apart basins. *Marine and Petroleum Geology*, 26(8), 1608–1623. <https://doi.org/10.1016/j.marpetgeo.2008.06.007>